Full Paper

Propellants, Explosives, Pyrotechnics

DOI: 10.1002/prep.202000314

Simulation of Heat Flow Curves of NC-Based Propellants – Part 1: Determination of Reaction Enthalpies and Other Characteristics of the Reactions of NC and Stabilizer DPA Using Quantum Mechanical Methods

Daniel G. Itkis[a] and Manfred A. Bohn*[a]

Dedicated to Dr. Norbert Eisenreich (1948–2019), scientist at Fraunhofer ICT

Abstract: The heat flow curves of nitrocellulose (NC)-based propellants are now an important assessment quantity for their quality and safety in storage and service. The measurable heat flow is the summarized effect of the rates of all the reaction heats of the reactions going on in the material. To get a detailed assessment instead the only global one requires knowing the heat flow parts caused by NC and by stabilizer reactions. For this, in turn, one needs to find the reaction enthalpies of the essential NC decomposition reactions and the stabilizer reactions at the temperature of the measurement of the heat flow. These data are not available in the literature. To get meaningful data it was necessary to use quantum mechanical calculations, here so-called DFT (density functional theory) methods, to screen the possible reactions by transition states and the energetic situation between educts and products. For the calculation of the reaction enthalpies and the transition states, the reactants were embedded in a polarizable continuum, which simulates the NC environment for the reactants in NC and for the stabilizer reactions. In addition, to calculate bond dissociation enthalpies of NC and of nitroglycerine a type of shell model was used called ONIOM ('**O**ur own **N**-layered **I**ntegrated molecular **O**rbital and molecular **M**echanics' model). The results from the determinations of reaction enthalpies are used in the second part of the publication.

Keywords: DFT calculations · transition states · NC decomposition · stabilizer reactions · reaction enthalpies

1 Introduction

The heat flow of NC-based propellants is determined mostly with isothermal microcalorimeters. Similar to DSC the sample is measured against a reference to minimize temperature fluctuations in the surrounding isothermal body, mostly a water or oil bath. Ideally, the reference side should have the same thermal mass as the sample side. This means heat capacity times mass should be nearly equal for both sides. Some of the modern equipment can measure even in the nW range per gram substance, and for this, the reference temperature bath must be kept constant in the range of 1E-5 to 1E-6 Kelvin. For more details see Supplemental Information. The measured heat flow (often between 10 and 300 μW/g) is a summation on all heat flow effects produced from all reactions occurring in the material, meaning all exothermal and endothermal effects are summed up. For the assessment of stabilizers, it is of interest to assign the parts of the gross heat flow to the individual reactions of NC and the stabilizer reactants. Also, physical effects may contribute, but these are not considered here and normally are not dominant during the measurements of NC-propellants.

For achieving the aim to simulate heat flow curves the necessary decomposition reactions of NC and the stabilizer reactions must be known, with their enthalpies of reaction. The decomposition reactions of NC and the stabilizer reactions have been extensively investigated. For NC mainly reaction products were identified, and many hypotheses exist about the detailed decomposition reactions. Many activation energies have been determined. The situation with stabilizers is better in that a lot of consecutive products were identified and most of them can be quantified today.

[a] *D. G. Itkis, M. A. Bohn*
Fraunhofer-Institut für Chemische Technologie (ICT), Joseph-von-Fraunhofer-Straße 7, 76327 Pfinztal, Germany
**e-mail: Manfred.Bohn@ict.fraunhofer.de*

Supporting information for this article is available on the WWW under https://doi.org/10.1002/prep.202000314

The point of interest here are reaction enthalpies, which are not known. Therefore, at first, the task was started to get the necessary insights and results, and the best way is probably to use the meanwhile well-developed quantum mechanical methods. They provide with the reaction paths via transition states and with the looked-for reaction enthalpies ΔH_R, reaction free Gibbs energies ΔG_R and the transition state (TS) data, and this all at the temperature of the applied measurements. Because the possible decomposition reactions of NC are very manifold, only some considerations could be made on reasonable ways of NC decomposition with their energetic reaction data. The nitration reactions of the stabilizer DPA are also discussed in literature. But the mechanisms are still hypotheses and not finally proven and reaction enthalpies are not given. For our objective, some reaction ways are taken to get the reaction energetic data and it is tried to get some light onto the reaction types. In the following the quantum mechanically (QM) based computational methods are described. For more explanations on these methods, the provided Supplemental Information, see section 7, may be useful. A short, concise review on NC and stabilizer reaction follows. In part 2 of this publication unit [1], the data obtained from this part 1 are used for the simulation of the heat flow curve of a DPA stabilized propellant.

2 Computational Methods

In this section, the so-called level of QM methods and newer developments are shortly described, see also the list of abbreviations and supplemental information. All calculations were performed with the (electron) **D**ensity **F**unctional **T**heory (DFT) as part from the Gaussian 2016 [2] program package. Geometries representing energetic minima and transition states (TS) of the pertinent compounds are optimized using the functional 'ωB97X-D' [3] and the basis set 'aug-cc-pvtz'. The ωB97X-D functional incorporates several notable improvements to the Becke 97 (B97) functional [4], namely a long-range correction and an empirical Grimme type dispersion [5], incorporated by the method shown in [3]. It has been found to provide low errors for the calculation of reaction enthalpies [6] and noncovalent interactions [7]. In this work, the convergence thresholds used in minimization calculations for energies, root mean square (RMS) forces, and RMS displacements were imposed at 10^{-6} H (Hartree, 1 H = 2625.50 kJ/mol), $5.67 \cdot 10^{-4}$ H/Å and $6.35 \cdot 10^{-4}$ Å, respectively.

The IEFPCM (**I**ntegral **E**quation **F**ormalism for the **P**olarizable **C**ontinuum **M**odel) solvation model [8] is applied to simulate the NC environment (here also called NC-continuum). It belongs to the so-called **S**elf-**C**onsistent **R**eaction **F**ield (SCRF) models. The IEFPCM method provides a polarizable continuum around the target molecule. In this way, intermolecular interactions via induced charges are included. For the value of the dielectric constant of this NC-continuum $\varepsilon_r = 7.0$ was chosen in agreement with experimental measurements [9]. The NC chain is simulated with three fully nitrated anhydroglucose (AHG) rings, see Figure 1, but in a so-called ONIOM configuration (**O**ur own **N**-layered **I**ntegrated molecular **O**rbital and Molecular **M**echanics) [10]. The chain ends are capped off with methoxy groups. Bond cleavages and rearrangements were limited to the central ring, while the outer two AHG ring units were included to consider the effects of the adjoining NC, sterically and otherwise.

In order to expedite computations, these outer rings were treated with the computationally less demanding BLYP functional and a double zeta 6-31 + + G(d,p) Pople-type basis set within the layered ONIOM. The central ring was computed with functional ωB97X-D and basis set aug-cc-pvtz. Frequency analyses are performed to verify the validity of each alleged minimum structure and the TS. Energetic minima have exclusively real frequencies, while a real TS is characterized as a saddle point with exactly one imaginary vibration frequency. This is the most encountered situation, there is only one way to products and the term saddle stands for a typical 'horse saddle'. But other transition regions are possible with several ways over a high valley into low energy levels. Sometimes the term 'monkey saddle' is used, which has two ways to products. In the TS the displacement vectors of the vibrational modes with an imaginary frequency are shown as blue arrows in the figures. Based on the frequency analyses, corrections are made to the electronic energies for zero-point energies. The temperature parts of the internal energy up to 80 °C (353.15 K) are considered via the partition functions of translation, rotation, and vibration for the enthalpies and Gibbs free energies (see also Supplemental Information). These data are used to predict the values of reaction enthalpies ΔH_R and reaction free Gibbs energies ΔG_R as well as the barrier values $\Delta H^{\neq}$ and $\Delta G^{\neq}$ to reach the TS.

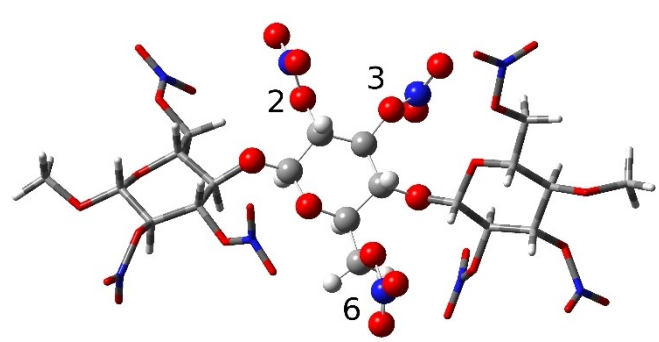

Figure 1. Geometry optimized minimum structure of the NC trimer in ONIOM configuration and in IEFPCM solvation. The central ring (ball-and-stick representation) is computed with ωB97X-D/aug-cc-pvtz, the outer rings (tube type representation) are treated with BLYP/6–31 + + G(d,p). The O–NO_2 positions on the central ring are indicated as 2, 3, and 6. Color code: oxygen in red, nitrogen in blue, carbon in gray, and hydrogen in white.

3 Short Overview on NC Decomposition and DPA Stabilizer Reactions

3.1 NC Decomposition Reactions

The literature on NC decomposition reactions is numerous. Here only a selected part is taken to get the wanted information on the decomposition behavior. A recommendable review on NC decomposition is provided by Brill and Gongwer [11]. This paper covers most of the knowledge and an analytically minded well-weighted assessment of the data is given. The main results for the decomposition in the temperature range up to 100 °C are summarized as follows. The start of the decomposition is seen as the homolytic splitting of the CO–NO_2 bond at temperatures about 50 °C to 100 °C, because it has a low bond dissociation enthalpy of about 160 to 170 kJ/mol, see also [12]. After this initial step rapid secondary reaction happens, which are autocatalytic, self-heating and cause breakdown of the NC backbone [13]. The autocatalytically active species, often called P in literature, are still not really known, but it is assumed they belong to the group NO_2, HNO_2, and HNO_3 and probably other aiding acidic compounds as formic acid and oxalic acid. The paper contains no information about reaction enthalpies, only a lot of activation energies were collected of some possible reactions, obtained with many methods.

The breakdown of the NC backbone can be followed by the polymer-analytical technique of gel permeation chromatography (GPC). The important point is that in spite of active stabilization the molar mass of NC decreases, this means stabilizer consumption and molar mass decrease go in parallel. This is documented for example in [14,15,16]. This means with the split-off of NO_2 from the nitrate ester groups in NC the cleavage of the NC backbone is initiated. To this fact, no detailed information is found in literature except the named one. Therefore, some thoughts were made to establish a reaction series that leads to NC chain scission, see Section 4. Because the work in [12] has considered only isolated molecules, a new effort was made to get more realistic data on bond dissociation enthalpies of the CO–NO_2 bonds in NC, as described in Section 2. Valuable detailed information on a decomposition of NC is compiled in [17,18]. In [19] an extensive work was conducted on low molecular mass nitrate esters (not on NC), but also interesting information is provided.

Special topics are treated in [20,21,22]. In [20] the decomposition of NC was followed by given off NOx and its concentration determination via chemiluminescence over the temperature range 22 °C and 147 °C. A two-stage decomposition was found with a transition temperature of about 92 °C. Below this temperature, the activation energy is 106.4 kJ/mol and above 178.8 kJ/mol. The higher value may be identified with the homolytic cleavage of CO–NO_2 bond as the rate-determining step, but the direct split-off of HNO_2 seems more probably in this case, see Section 4.1.2. The low activation energy is not yet clearly assignable, maybe secondary reactions must be taken into consideration. A possibility could be the decomposition of peroxo nitrites formed intermediary by recombination of NO_2 to the CO-radical to form CO–ONO. Such possibility was postulated in [21]. In [12] the bond dissociation enthalpy of peroxo nitrate, CO-ONO_2 was found to be about 93 kJ/mol. In [22] activation energies are discussed for the intrinsic NC decomposition as CO–NO_2 splitting with Ea-value of 150.6 kJ/mol and for the autocatalytic decomposition with Ea = 192 kJ/mol. But the last value seems too high, because autocatalytic behavior happens markedly only, when the corresponding activation energies are lower than the first-order decomposition value producing the autocatalytically effective product, here generally named P. Another possibility would be an exceptional high pre-exponential factor to get the autocatalysis reaction into play.

3.2 DPA Stabilizer Reactions

The reactions of stabilizer DPA have been looked at already quite often. But in all these investigations no reaction enthalpies were determined. Only for one reaction, namely the nitrosation of DPA by HNO_2 to NNO-DPA + H_2O, a value could be found as $\Delta H_R = -62.8$ kJ/mol [23]. The determination dates back to more than 110 years. At first, we look at the stabilizing reactions of DPA. Generally, it is now agreed that it binds NO_2 and in part NO, which interrupts the autocatalytic decomposition channel of NC. But it cannot stop the intrinsic decomposition of the NC, which continues and therefore consumes stabilizer, together with chain splitting of the NC, which is also part of its intrinsic decomposition. The papers in the literature can be divided mainly into two groups: one group deals with the determination of consecutive products of DPA, qualitatively and quantitatively, the last may be used for in-service time prediction and kinetic modeling. The other group tries to find out the reaction mechanisms, this means what are the details of the reactions between DPA and NO_2, NO, HNO_2, HNO_3.

To the first group belong [24,25,26,27,28]. In part also some considerations are given on reaction mechanisms in these references. In [24] extensive work and effort was made to elucidate the series of reaction products of several stabilizers, such as DPA, 2-nitro-DPA, EC (ethyl centralite), Akardite I and Akardite II (Ak II). Investigated was the time to autocatalysis at temperatures between 65 °C and 90 °C with 5 °C interval employing mass loss measurements. The beginning of autocatalysis is seen as the beginning of the strong increase in mass loss, which starts after the total loss of any stabilization as important prerequisite. These times to autocatalysis correlated well and activation energies were obtained. With DPA a value of 138.9 kJ/mol was found. In [25,26] the consecutive products of DPA were determined by HPLC (High-Performance Liquid Chromatog-

raphy). The typical series were found. In [26] several single-base propellants were investigated. Starting stabilizers have been: DPA, 2-nitro-DPA, 4-nitro-DPA and NNO-DPA. The relative concentration courses and ratios were different for the propellants. A final reason for this could not be identified and the conclusion is that every propellant has its own characteristic. In [27] the decrease of typical stabilizers DPA, EC, Ak II and MNA (N-Methyl-p-Nitroaniline) during aging in individual samples was investigated in model propellants of type triple base M30-A1 containing about 28 mass-% NC, 21-mass-% NG and 49 mass-% nitroguanidine. In parallel, the heat flows were determined. The correlations between both quantities are shown and discussed. The concentration courses of the DPA consecutive products obtained by the aging of a single base propellant were determined up to triply nitrated DPAs in [28]. The aim was to model them with extended reaction kinetic schemes to get the individual reaction rate constants. Several kinetic schemes were established and applied.

The next two papers [29] and [30] tried to elucidate the reactions of stabilizer DPA with NO_2. Different concepts were used: in [29] the stabilizers were applied as films on glass plates and the increase in mass was used to determine the progress of the reactions between stabilizer DPA, NNO-DPA, nitrated DPAs (2-nitro-DPA, 4-nitro-DPA 2,4-DN-DPA, 2,4′-DN-DPA), and the gases NO_2 and NO. It was found that NO did not react with NNO-DPA, 2-nitro-DPA, 2,4-nitro-DPA in this experimental arrangement. In [30] the stabilizer was mixed with fluffy cellulose and then NO_2 was added in portions. The next portion was added after the complete disappearance (assessed just by eye) of NO_2 from the foregoing injection. The occurrence and courses of the DPA and its consecutive products were analyzed by HPLC. Typical courses were obtained similar to the ones revealed by propellant aging, but as a function of NO_2 addition, not as a function of direct time. Four substances were used as starting stabilizers: DPA, NNO-DPA, 2-NO_2-DPA, and 4-NO_2-DPA. It was demonstrated that nitrogen dioxide vapor in contact with a solid-solid phase containing cellulose and DPA or NNO-DPA or 2-NO_2-DPA or 4-NO_2-DPA, causes two types of reactions with the stabilizer molecules: N-nitrosation and C-nitration. The N-nitrosation seems the favored reaction since a resonance stabilized radical intermediate is produced. C-nitration proceeds at a lower rate than N-nitrosation since it involves additional energy to bring the resonance energy stabilized aromatic system in a reactive transition state. It could be not clarified, what type of reactions occur to achieve at C-nitration: radical substitution or the ionic aromatic electrophilic substitution. A nitration of DPA at ring position 3 was not revealed.

In [31] implications were found, because not all DPA stabilizer content could be extracted from the propellant. It was discussed that DPA can be bonded to nitrocellulose, via radical reactions. Probably also other stabilizers could be bonded in a similar way to NC. The work of [32] tried to find out information about the radical reactions by determining the free radical concentrations by ESR (Electron Spin Resonance). Generally, the free radical density increases with decreasing DPA. The free radical density reaches a peak point and starts to decrease when DPA is depleted to near zero. Correlations between heat flow curve, stabilizer depletion and free-radical distribution have been discussed. The authors assume an intramolecular reaction mechanism of N-NO-DPA (N-nitroso-DPA) or N-NO_2-DPA (N-nitro-DPA) to the C-nitrated species. In this way, the NO or NO_2 cannot re-interact with the NC and NG again during the rearrangement process, which would be the wished situation. If the rearrangement is intermolecular, the C-nitration reaction is of type aromatic electrophilic substitution. Finally, the conclusion is: The degradation mechanism of nitrate ester NC and NG with stabilizer DPA is very complex. Whether the mechanism follows either the ionic, free radical, or charge transfer complex pathway or all of them, depends upon the acidity and humidity of the composition and the structure of the stabilizer.

4 Decomposition Reactions of NC and their Thermodynamic Data

4.1 Nitrate Ester Decomposition

4.1.1 Homolytic CO–NO_2 Bond Cleavage

It is generally assumed that the first step in the degradation of NC at higher temperatures consists of a thermally facilitated homolytic split of the relatively weak RO–NO_2 bond of one of the nitrate ester groups, thereby producing two radicals:

$$R{-}O{-}NO_2 \rightarrow R-O\cdot + \cdot NO_2$$

This intrinsic first-order reaction is unaffected by the presence of stabilizers. It can be possible that good gelatinization of the NC by the stabilizer change somewhat the dissociation behavior. This is a hypothesis at time. Using the trimer model shown in Figure 1, bond dissociation enthalpies $\Delta_{bond}H$ and bond dissociation Gibbs free energies $\Delta_{bond}G$ were computed in two ways. The minimum energy structure of the fully nitrated trimer structure is geometry optimized and used always as a reference. Relative to this reference, the minimum energy structure of the formed NC radical after the loss of NO_2 radical is considered differently. In a real NC chain, it can be assumed that the possibility of a given section to adjust or contract sterically in response to chemical changes is strongly hindered in comparison to the trimer model. Accordingly, two situations are considered here for the estimate: (I) a completely relaxed, i.e. separately optimized structure for the alkoxy radical products; (II) a completely 'unrelaxed' geometry of the alkoxy radicals.

In the second case the optimized trimer educt structure is not modified after removing the NO_2-radicals, thereby

blocking any geometry changes after the bond scission. The unrelaxed situation is seen as a borderline case corresponding to an immobilized NC chain. These two estimates give a range of expected bond dissociation enthalpies and Gibbs energies, see Table 1. The same procedure was used to calculate the dissociation data of the CO–NO_2 bonds in nitroglycerine (NG), but here only with relaxed NG radical. Two environments are chosen in the solvation model: NG in NG with $\varepsilon_r = 19.3$ and NG in NC with $\varepsilon_r = 7.0$.

Table 1. Computed O–NO_2 bond dissociation enthalpies and bond dissociation Gibbs free energies for relaxed (optimized) and unrelaxed alkoxy radicals in kJ mol^{-1} at 80 °C computed with the ONIOM trimer shown in Figure 1. Calculation with IEFPCM, NC in NC-continuum, NG in NG-continuum, and NG in NC-continuum.

	After NO_2 split-off, the alkoxy radicals are			
	unrelaxed		relaxed	
NC in NC, $\varepsilon_r = 7.0$				
Position	$\Delta_{bond}H$	$\Delta_{bond}G$	$\Delta_{bond}H$	$\Delta_{bond}G$
2	161.7	123.1	150.2	87.6
3	164.9	115.0	157.8	96.3
6	160.7	107.1	153.9	87.2
NG in NG, $\varepsilon_r = 19.3$				
1, 3	–	–	164.0	90.5
2	–	–	158.7	83.6
NG in NC, $\varepsilon_r = 7.0$				
1, 3	–	–	164.0	91.8
2	–	–	159.0	86.3

4.1.2 Elimination of Nitrous Acid

Instead of the formation of NO_2 it is conjectured that nitrous acid, HNO_2, can be produced directly:

$$RH{-}O{-}NO_2 \rightarrow TS \rightarrow R{=}O + HNO_2$$

This reaction is a type of monomolecular elimination and involves a five-membered transition state and leaves behind an aldehyde or a ketone group. At this point, a remark is stated: such elimination has been found to be the energetically most favorable decomposition pathway for some nitramines like methylene nitramine and with RDX in the gas phase. In both cases, the activation energy for this elimination was lower than the N–NO_2 bond dissociation energy [33,34]. With NC, the formation of these carbonyl compounds by HNO_2 elimination is well documented for the basic hydrolysis of NC, which yields nitrite salts and carbonyl compounds as the main products [35]. Thus, this pathway is proposed as an alternative to the homolytic O–NO_2 bond cleavage. In Figure 2, the educt, the TS, and the product are shown, the ordinate is the Gibbs free energy at 80 °C relative to the educt. The data of HNO_2 elimination from NC are given in Table 2 for 80 °C for the relaxed case.

Table 2. Computed TS activation and reaction enthalpies and Gibbs free energies for HNO_2 elimination in kJ mol^{-1} at 80 °C computed with the ONIOM trimer shown in Figure 1. Always relaxed species.

Position	TS		Products	
	$\Delta H^{\neq}$	$\Delta G^{\neq}$	ΔH_R	ΔG_R
2	177.9	173.8	−77.5	−145.3
3	181.9	186.9	−93.7	−158.6
6	183.7	178.7	−69.5	−133.4

This leads to an interesting consequence: One can reasonably assume the TS for the CO–NO_2 bond splitting has the same thermochemical data as the dissociation data given in Table 1. Therefore, the homolytic NO_2 formation is lower in activation energy and thus is ostensibly more prevalent. But it is thermodynamically unfavorable because it is very endergonic. The reverse reaction, i.e. rebinding of NO_2 radical is thermodynamically favorable and readily takes place. There is also reason to suppose that the generated NO_2 in the rigid framework of the NC strands remains in the proximity of the cleavage site for a period of time, while repeatedly rebinding and breaking the O–NO_2 bond [36]. Since the elimination of HONO is irreversible, it may contribute to the initial stages of NC degradation more than the reversible, thermodynamically unfavorable homolytic cleavage. Thus, a compelling case can be made for an alternative first step of NC decomposition. However, because of the higher activation energy of the HNO_2 elimination, this reaction comes to an advantage with increasing temperature.

4.2 Further Decomposition of NC

From section 3.1 it is known that with the split-off of NO_2 or HNO_2 the backbone of NC suffers from chain cleavage. The remaining NC chain further breaks down leading to the generation of more oxides of nitrogen, various carbonyl compounds, carbon oxides, and many other fragments. The presence of reactive species, including NO_2 and HNO_2, also promotes the further degradation of NC in an autocatalytic manner.

A great amount of different degradation pathways with divergent product combinations and thermodynamic data can be envisioned for these further decomposition steps. We have concentrated on one such pathway with the aim of attaining realistic products and an estimate of possible reaction enthalpy values, see Figure 3 and Reaction Scheme 1. The intermediate alkoxy radical (b$^{\bullet}$) produced by

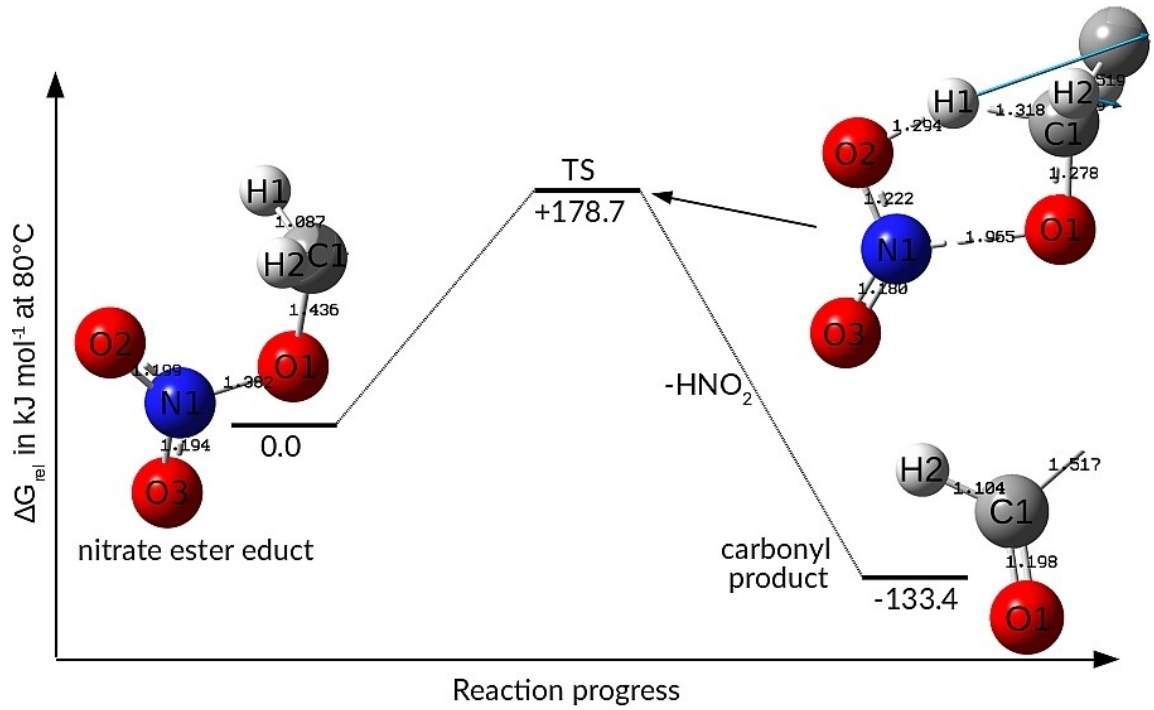

Figure 2. Gibbs free energy, relative to the educt, along with the reaction coordinate for the HNO_2-elimination at the 6-position of nitrocellulose and optimized structures of the relevant part of the educt. The atom numbering is reduced to this part without referring to the ring numbering of the NC. Data are shown for 80 °C. The Table 2 contains the data at 80 °C for all three ring positions. The blue arrows (one long and one short) on the right above show the displacement vectors of the imaginary vibration of the transition state (TS) structure. Bond lengths in Angström. The formed product is very exergonic.

the cleavage of the O–NO_2 bond of the 2-position of the trimer (a) further degrades via an additional loss of $^{\bullet}NO_2$ from the 3-position and forms the double radical (b$^{\bullet\bullet}$); simultaneously, glyoxal $C_2H_2O_2$ is eliminated. This process already ruptures the NC chain, leading to two products (as end group situation of the two chain fragments): a formate ester (d) and an intermediate (c) with an allyl structure. The former anhydroglucose unit is gradually destroyed as it progresses from the allyl radical stage (c) by losing $^{\bullet}NO_2$ to form a vinyl radical intermediate (e$^{\bullet}$). This vinyl radical is unstable and splits off CH_2O and at the remaining radical position a former released $^{\bullet}NO_2$ takes a H radical. Therewith an alkyne type product (f) with a C–C triple bond and HNO_2 are formed. The formate ester (d) can further degrade, see Figure 3, on the left-middle of the structure (d) we have the group O=CH–O–C(ring), yielding an alcohol group HO–C-(ring) by splitting off CO. The reaction enthalpies at 80 °C determined with IEFPCM and NC-continuum are shown in Reaction Scheme 1. The indication of radical functions is shown with a dot.

Reaction Scheme 1

$(a) \rightarrow (b\cdot) + \cdot NO_2$

with $\Delta H_R = +150.2\,kJ\,mol^{-1}$

$(b\cdot) \rightarrow (b\cdot\cdot) \rightarrow (c) + (d) + \cdot NO_2 + C_2H_2O_2$

with $\Delta H_R = -105.1\,kJ\,mol^{-1}$

$(c) \rightarrow (e\cdot) + \cdot NO_2$

with $\Delta H_R = +173.1\,kJ\,mol^{-1}$

$(e\cdot) + \cdot NO_2 \rightarrow (f) + HNO_2 + CH_2O$

with $\Delta H_R = -37.9\,kJ\,mol^{-1}$

$(d) \rightarrow ROH + CO$

with $\Delta H_R = +31.5\,kJ\,mol^{-1}$

The net reaction of reactions (1) to (5) is exergonic:

$C_6H_7O_2(ONO_2)_3 \rightarrow C_2H_2O_2 + ROH + CO +$

$RO{-}C \equiv CH + 2NO_2 + HNO_2 + CH_2O$

with $\Delta H_R = +211.7\,kJ\,mol^{-1}$ and $\Delta G_R = -243.4\,kJ\,mol^{-1}$.

The net reaction enthalpy and Gibbs free energy for this overall decomposition reaction are $\Delta H_R = +211.7\,kJ\,mol^{-1}$ and $\Delta G_R = -243.4\,kJ\,mol^{-1}$ per anhydroglucose ring. This breakdown reaction course is endothermal but exergonic. However, it needs to be noted that several of the proposed products are anticipated to further degrade. For instance, a redox reaction between the oxidizing agent NO_2 and re-

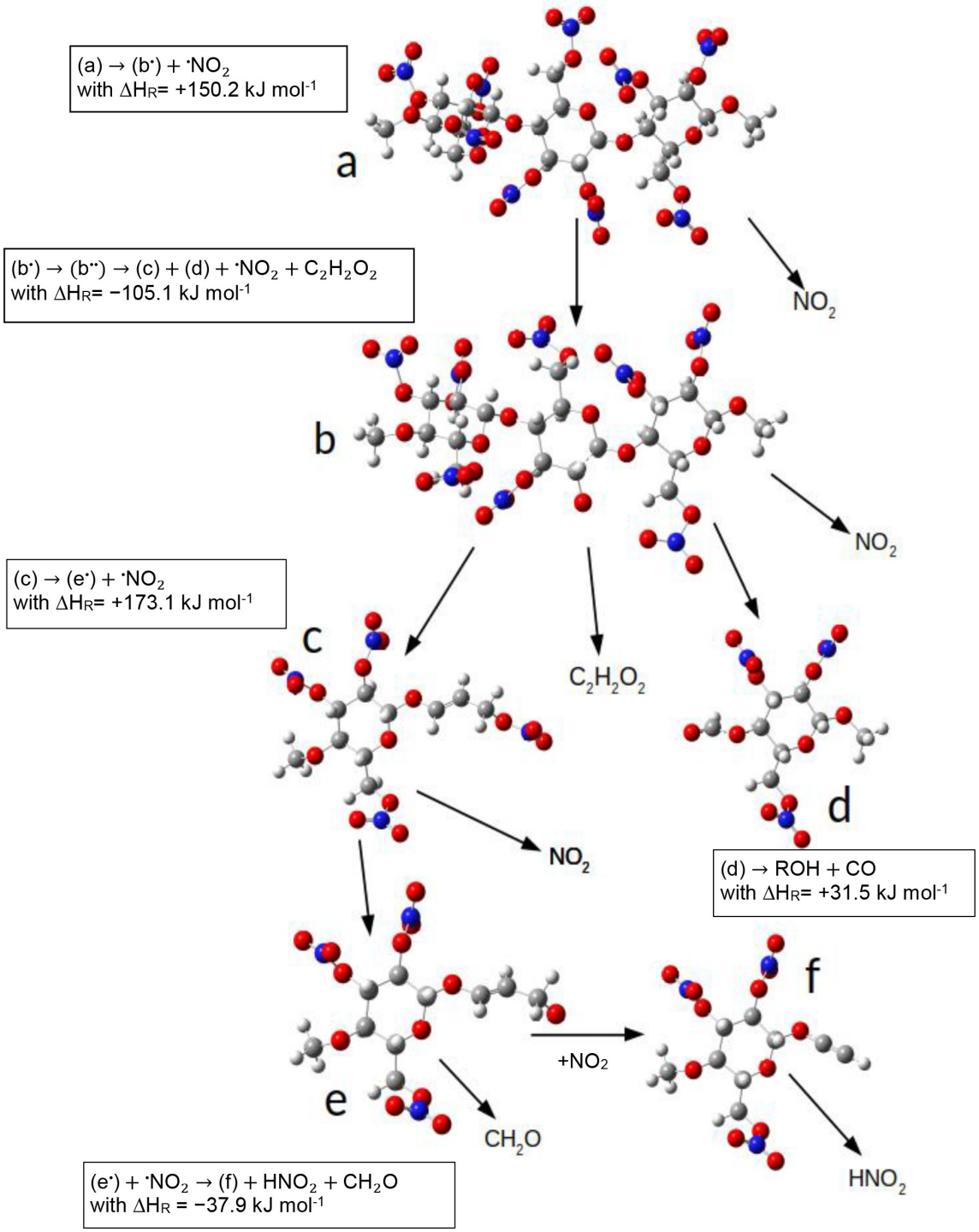

Figure 3. Proposed degradation mechanism of NC with optimized intermediates and product structures as parts of the ONIOM trimer model. The shown reaction enthalpies are at 80 °C.

ducing agent formaldehyde can liberate a large amount of heat:

$$C_6H_7O_2(ONO_2)_3 \rightarrow C_2H_2O_2 + ROH + CO + RO{-}C \equiv CH + 2NO + HNO_2 + H_2O + CO_2$$

with $\Delta H_R = -175.8\,kJ\,mol^{-1}$ and $\Delta G_R = -668.4\,kJ\,mol^{-1}$.

With this secondary reaction, the new values for the reaction enthalpy and reaction Gibbs free energy are $\Delta H_R = -175.8\ kJ\,mol^{-1}$ and $\Delta G_R = -668.4\ kJ\,mol^{-1}$ per anhydroglucose unit and the decomposition turns to become already exothermal and is now very exergonic.

5 Reactions of NC Degradation Products with Diphenylamine and their Thermodynamic Data

DPA is routinely used as a stabilizer to prolong the in-service time of NC based propellants. Its function is based on its ability to bind the autocatalytically active decomposition products of NC and render them innocuous. This is most conspicuously with NO_2, HNO_2, and HNO_3, although other compounds have been suggested to play a role as well [31,37]. The main products of these reactions have been identified as N-nitroso-DPA (NNO-DPA), 2-nitro-DPA ($2NO_2$-DPA), 4-nitro-DPA ($4NO_2$-DPA), see Figure 4. But further products with multiple nitro groups can be found with the increasing aging of the material. As already stated in section 3.2, it is not clear in full by what types of mechanisms these compounds are generated [32,37,38]. Here it is tried to give some possible explanations.

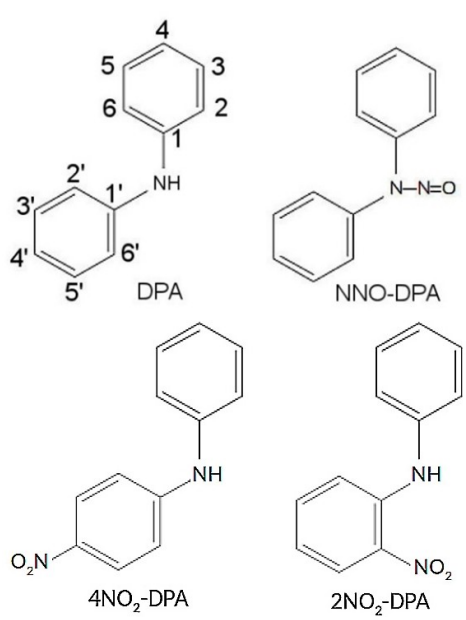

Figure 4. DPA and some of its first-step products resulting from stabilizing reactions in NC based propellants. Above: diphenylamine, N-nitroso diphenylamine. Below: 4 -nitro-diphenylamine, 2-nitro-diphenylamine. With the DPA formula, the atomic positions used later are shown.

5.1 Direct Radical Substitution

DPA has essentially four reactively/chemically different positions bearing hydrogen atoms, which could be involved in substitution reactions: N, 2, 3, and 4 as shown in Figure 4; positions 5 and 6 are equivalent to 3 and 2, respectively. One way to assess the reactivity of these positions is to compute and compare the homolytic bond dissociation enthalpies as shown in Table 3. The N–H bond is the weakest, while the three C–H bonds are about 110 $kJ\,mol^{-1}$ stronger and within 1% equal to each other. This implies that the N-position in DPA should be the most reactive by a wide margin and attacked preferentially over the other positions in most reactions.

In other words, the secondary amine group is particularly prone to the abstraction of the H atom by radicals. A reaction yielding NNO-DPA can be written in two steps as shown in Reaction Scheme 2; Ph indicates phenyl. The thermodynamic data for these three reactions were calculated with surrounding the NC-continuum, results are given in Table 4.

Reaction Scheme 2

$$DPA + \dot{N}O_2 \rightarrow Ph{-}\dot{N}{-}Ph + HNO_2 \quad (I)$$

$$Ph{-}\dot{N}{-}Ph + \dot{N}O \rightarrow NNO - DPA \quad (II)$$

$$\text{In total}: \ DPA + \dot{N}O_2 + \dot{N}O \rightarrow NNO - DPA + HNO_2$$

5.2 Indirect Radical Substitution

As the bond dissociation enthalpies for the aromatic C–H bonds are too large for direct H abstraction, an indirect mechanism is proposed. First, an abstraction of hydrogen from DPA by NO_2 from the N–H takes place as shown in reaction (I) of Reaction Scheme 2. The resulting secondary

Table 3. Computed N–H and C–H bond dissociation enthalpies $\Delta_{bond}H$ in DPA at 80 °C. Molecules positioned in NC-continuum.

Position of H	N	2	3	4
Δ_{bond} H [$kJ\,mol^{-1}$]	357.4	471.1	465.8	471.2

Table 4. Computed reaction enthalpies ΔH_R and reaction Gibbs free energies ΔG_R in $kJ\ mol^{-1}$ for the two-step formation of NNO-DPA at 80 °C, reaction Scheme 2.

Reaction	ΔH_R	ΔG_R
(I)	34.3	35.5
(II)	−121.6	−63.3
total	−87.3	−27.8

aromatic amino radical is stabilized by the extensive resonant delocalization of the unpaired electron, particularly to the ortho and para positions of the aromatic rings. The recombination of this unpaired electron with one more moiety of NO_2 is therefore not confined to the amino position. The products of the addition of NO_2 to the phenyl ring are tautomers and precursors to the nitro-DPA's which can re-aromatize through a proton migration from the C-position to the N-position, maybe similar to one of HAT mechanisms (hydrogen atom transfer mechanism), here in the intramolecular version [39,40,41]. Anyway, the driving force for any type of H migration is to retain the resonance energy of the aromatic ring. The overall reaction is written in three steps, see Reaction Scheme 3. The structures of all reactants are optimized in NC-continuum. The tautomer intermediates are shown in Figure 5. Structure (c) in Figure 5 shows the energetic minimum of the meta substituted intermediate. The meta substitution is thermochemical less favored but possible, as seen from the final energetic reaction values. However, the addition of a NO_2 molecule to the 3-position of one of the aromatic rings leads to the formation of a new bond between two of the ring's carbon atoms.

Reaction Scheme 3

$$\mathrm{DPA} + \dot{\mathrm{N}}\mathrm{O}_2 \rightarrow \mathrm{Ph}{-}\dot{\mathrm{N}}{-}\mathrm{Ph} + \mathrm{HNO}_2 \qquad \text{(Ia)}$$

ortho substitution:

$$\mathrm{Ph}{-}\dot{\mathrm{N}}{-}\mathrm{Ph} + \dot{\mathrm{N}}\mathrm{O}_2 \rightarrow 2\mathrm{NO}_2{-}\mathrm{DPA} - \text{tautomer} \qquad \text{(IIa)}$$

$$2\mathrm{NO}_2{-}\mathrm{DPA} - \text{tautomer} \rightarrow 2\mathrm{NO}_2{-}\mathrm{DPA} \qquad \text{(IIIa)}$$

para substitution:

$$\mathrm{Ph}{-}\dot{\mathrm{N}}{-}\mathrm{Ph} + \dot{\mathrm{N}}\mathrm{O}_2 \rightarrow 4\mathrm{NO}_2{-}\mathrm{DPA} - \text{tautomer} \qquad \text{(IIb)}$$

$$4\mathrm{NO}_2{-}\mathrm{DPA} - \text{tautomer} \rightarrow 4\mathrm{NO}_2{-}\mathrm{DPA} \qquad \text{(IIIb)}$$

meta substitution:

$$\mathrm{Ph}{-}\dot{\mathrm{N}}{-}\mathrm{Ph} + \dot{\mathrm{N}}\mathrm{O}_2 \rightarrow 3\mathrm{NO}_2{-}\mathrm{DPA} - \text{tautomer} \qquad \text{(IIc)}$$

$$3\mathrm{NO}_2{-}\mathrm{DPA} - \text{tautomer} \rightarrow 3\mathrm{NO}_2{-}\mathrm{DPA} \qquad \text{(IIIc)}$$

The meta tautomer is a substituted bicyclo[3.1.0]hex-2-ene and the loss of aromaticity is irreversible. This structure is with $\Delta G_R = +95.2\ \mathrm{kJ\,mol^{-1}}$ (reaction IIc) strongly unfavorable. The reaction (IIIc) in Scheme 3 and Table 5 is purely hypothetical and formally included. On the other hand, ortho and para substitutions of these tautomer types are residually resonance-stabilized, energetically favorable, and likely to proceed. The lack of a meta intermediate with low activation energy can account for the lack of a meta substituted nitro-DPA in the substitution pattern of DPA and therefore experimentally not observed. In conclusion, a radical substitution mechanism is possible and can explain the typical consecutive products of DPA.

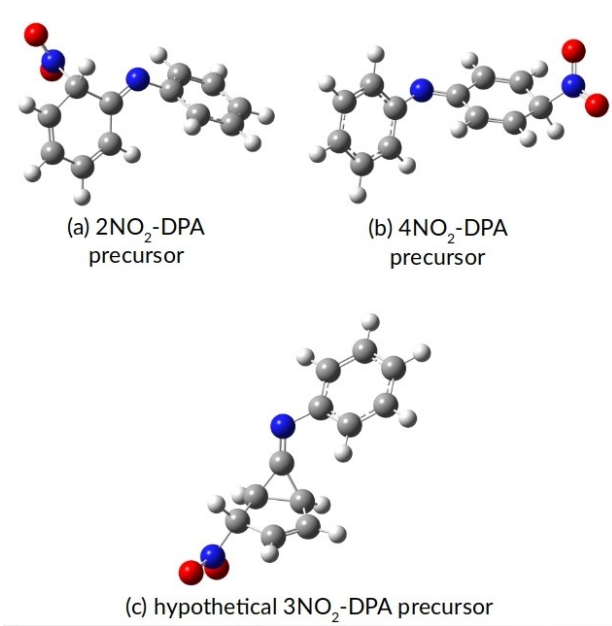

Figure 5. Optimized structures of the tautomers of nitro-DPA's, which are proposed to exist as intermediates during a radical substitution by NO_2.

Table 5. Computed reaction enthalpies ΔH_R and Gibbs free energies ΔG_R in $\mathrm{kJ\,mol^{-1}}$ at 80 °C for radical type nitration of DPA according to reaction Scheme 3.

	ΔH_R	ΔG_R
(I)	+34.3	+35.5
(IIa) ortho tautomer	−61.4	−1.0
(IIIa) ortho NO_2-DPA	−135.4	−127.9
ortho total (I + IIa + IIIa)	−162.5	−93.4
(IIb) para tautomer	−73.6	−11.6
(IIIb) para NO_2-DPA	−133.0	−129.6
para total (I + IIb + IIIb)	−172.3	−105.7
(IIc) meta tautomer	+31.6	+95.2
(IIIc) meta NO_2-DPA	−226.4	−226.8
meta total (I + IIc + IIIc)	−160.5	−96.1

5.3 Aromatic Electrophilic Substitution

Aromatic nitrations by nitronium sources are archetypal exemplifications of electrophilic aromatic substitutions ($S_{E,Ar}$). It stands to argue that an $S_{E,Ar}$ mechanism may be responsible for the nitration of the aromatic rings of DPA in the

propellant environment. This proposition is also in concord with the experimental substitution pattern of ortho/para direction as it is expected from an aromatic amine. The nitrating agent for this pathway is primarily nitric acid formed by the hydrolysis of nitrate ester groups, the disproportionation of nitrous acid or the oxidation of other nitrogen-containing compounds by atmospheric oxygen. The net substitution reactions to the mono-nitro-DPA are written as:

$$\text{ortho}: \text{DPA} + \text{HNO}_3 \rightarrow 2\ \text{NO}_2\text{–DPA} + \text{H}_2\text{O}$$

$$\text{para}: \text{DPA} + \text{HNO}_3 \rightarrow 4\ \text{NO}_2\text{–DPA} + \text{H}_2\text{O}$$

Alternatively, N_2O_5 can be formed in anhydrous conditions from nitric acid in the reaction:

$$2\ \text{HNO}_3 \rightleftharpoons \text{N}_2\text{O}_5 + \text{H}_2\text{O}$$

It acts as the nitronium source This reaction has been computed to have only $\Delta H_R = +59.4\ \text{kJ mol}^{-1}$ and $\Delta G_R = +58.6\ \text{kJ mol}^{-1}$. For nitrations with N_2O_5 the reaction equations can be written as:

$$\text{ortho}: \text{DPA} + \text{N}_2\text{O}_5 \rightarrow 2\ \text{NO}_2\text{–DPA} + \text{HNO}_3$$

$$\text{para}: \text{DPA} + \text{N}_2\text{O}_5 \rightarrow 4\ \text{NO}_2\text{–DPA} + \text{HNO}_3$$

The thermodynamic data for these reactions to the two mono-nitro-DPA are summarized in Table 6. The reactions are very exotherm and exergonic and can promote the formation reaction of N_2O_5.

Table 6. Computed reaction enthalpies ΔH_R and reaction Gibbs free energies ΔG_R for electrophilic aromatic nitrations of DPA to the mono-nitro-DPA in kJ mol^{-1} at 80 °C. All reactants in NC-continuum.

	with HNO_3		with N_2O_5	
Position	ΔH_R	ΔG_R	ΔH_R	ΔG_R
ortho	−125.0	−115.6	−184.4	−174.2
para	−134.8	−128.0	−194.3	−186.6

5.4 Compilation of Enthalpies and Gibbs free Energies for the Considered Reactions

The calculated reaction enthalpies and reaction Gibbs free energies for all pertinent reactions are compiled in Table 7 together with the considered reactions. These can be used alongside kinetic models following the concentrations of the stabilizer and its derivatives to model the heat flow curves of decomposing NC stabilized by DPA. The chosen reaction enthalpies for the modeling in part 2 are listed in Table 8. The reaction enthalpy values given for the intrinsic and autocatalytic NC decomposition are values in between a wide span from −90 to +160 kJ/mol, depending on what reaction is considered as the initial decomposition step. These values will be adjusted during the simulation of the heat flow curve by the fit algorithm. In principle, all the reaction enthalpy values of Table 8 should be seen as start values for the calculations. More on this will be given in part 2 [1].

5.5 The Autocatalytically Effective Species

Finally, some remarks on the nature of the autocatalytically effective species in NC decomposition are brought forward, which is commonly called just P. This P refers to several products of NC decomposition, which are treated formally as one 'global' reactant in kinetic modeling. It is a common opinion, that one of the first steps in the decomposition of NC is the homolytic split-off of radical NO_2. This radical is quite reactive and is mostly effective as H radical abstractor. It may abstract an H atom from the NC framework to form HNO_2, which can be involved in several reactions with the stabilizer. The most susceptible H types in NC are those on the C-atoms with a nitrate ester group. The abstraction of an H causes stabilization actions on this part of NC. This can be achieved by split-off of the corresponding NO_2 and formation of a carbonyl group O=C. The action of NO_2 has therewith produced a further NO_2, meaning a type of autocatalytic reaction propagation has happened. Further decomposition may proceed similarly according to Figure 3. This reaction behavior is quite probable what can happen under oxygen-free conditions. Already with small amounts of oxygen influence, the HNO_2 is oxidized to HNO_3. The formation of HNO_3 is most effective when water is present in small amounts. With higher water contents caused by increasing NC decomposition and together with some oxygen, nearly all of the NO_2 is converted to HNO_3 and this species is then the dominating autocatalytic one.

6 Summary and Conclusions

The survey on the reaction behavior of NC and the stabilizer DPA revealed that no reaction enthalpies were reported in the literature until this point. The start of decomposition of NC is generally accepted to be the homolytic thermolysis of one of the CO–NO_2 bonds because they have quite a low bond dissociation enthalpies in the range of 160 kJ/mol. The then following decomposition reactions lead to the destruction of the affected chain elements and a molar mass decrease of NC happens. This cannot be stopped by the typical stabilizers. The action of stabilizers prevents the autocatalytic decomposition of NC by chemically binding the autocatalytic species P, which is assumed to comprise NO_2, HNO_2, and HNO_3. The mechanism of the binding reaction between DPA and NO_2 and NO is not finally decided, but the indirect radical substitution for the C-nitration is prob-

Table 7. Reaction enthalpies ΔH_R and reaction Gibbs free energies ΔG_R in kJ mol^{-1} of the considered reactions at 80 °C. All calculations with IEFPCM to simulate NC-continuum environment for the reactants. Reactants optimized with DFT using functional ωB97X-D and as basis set aug-cc-pvtz.

No	Reaction type	ΔH_R	ΔG_R	remarks
	Homolytic splitting of bond CO-NO_2 in ONIOM-NC			
1	ONIOM-NC position 2 ⟶ $^{\bullet}NO_2$ + alkoxy radical position 2	+150.2 / +161.7; ΔH_R relaxed / unrelaxed		
2	ONIOM-NC position 3 ⟶ $^{\bullet}NO_2$ + alkoxy radical position 3	+157.8 / +164.9; ΔH_R relaxed / unrelaxed		
3	ONIOM-NC position 6 ⟶ $^{\bullet}NO_2$ + alkoxy radical position 6	+153.9 / +160.7; ΔH_R relaxed / unrelaxed		
	HNO_2 elimination, aldehyde product on residual NC body			activation parameters $\Delta H^{\ddagger}$ / $\Delta G^{\ddagger}$
4	ONIOM-NC position 2 ⟶ HNO_2 + aldehyde on position 2	-77.5	-145.3	+177.9 / +173.8
5	ONIOM-NC position 3 ⟶ HNO_2 + aldehyde on position 3	-93.7	-158.6	+181.9 / +186.9
6	ONIOM-NC position 6 ⟶ HNO_2 + aldehyde on position 6	-69.5	-133.4	+183.7 / +178.7
7	ONIOM-NC + $^{\bullet}NO_2$ ⟶ many reaction pathways	+60 to -246	-	autocatalytic reactions
	Formation of amino radical and ring radicals on DPA			
8	DPA + $^{\bullet}NO_2$ ⟶ $^{\bullet}$N-diphenyl +HNO_2	+34.3	+35.5	N-position
9	DPA + $^{\bullet}NO_2$ ⟶ $^{\bullet}$2-DPA +HNO_2	+148.1	+144.4	Ortho-position
10	DPA + $^{\bullet}NO_2$ ⟶ $^{\bullet}$3-DPA +HNO_2	+142.8	+139.9	Meta-position
11	DPA + $^{\bullet}NO_2$ ⟶ $^{\bullet}$4-DPA +HNO_2	+148.1	+143.9	Para-position
12	DPA + HNO_2 ⟶ $^{\bullet}$N-diphenyl + $^{\bullet}$NO +H_2O	+70.9	+18.8	N-position
13	DPA + HNO_2 ⟶ $^{\bullet}$2-DPA + $^{\bullet}$NO +H_2O	+184.6	+127.7	Ortho-position
14	DPA + HNO_2 ⟶ $^{\bullet}$3-DPA + $^{\bullet}$NO +H_2O	+179.4	+123.2	Meta-position
15	DPA + HNO_2 ⟶ $^{\bullet}$4-DPA + $^{\bullet}$NO +H_2O	+184.6	+127.2	Para-position
	Formation of x-N-DPA tautomers, H on the substitution position moves via H-shift to N			
16	$^{\bullet}$N-diphenyl + $^{\bullet}NO_2$ ⟶ 2-NO_2-DPA-tautomer ⟶ 2-NO_2-DPA	-61.4	-1.0	H shift ΔH_R /ΔG_R: -135.4 / -127.9
17	$^{\bullet}$N-diphenyl + $^{\bullet}NO_2$ ⟶ 3-NO_2-DPA-tautomer ⟶ 3-NO_2-DPA	+31.6	+95.2	H shift ΔH_R /ΔG_R: -226.4 / -226.8
18	$^{\bullet}$N-diphenyl + $^{\bullet}NO_2$ ⟶ 4-NO_2-DPA-tautomer ⟶ 4-NO_2-DPA	-73.6	-11.6	H shift ΔH_R /ΔG_R: -133.0 / -129.6
	Formation of mono-nitro-DPA with $^{\bullet}NO_2$ radical			
19	DPA+ 2 $^{\bullet}NO_2$ ⟶ 2-NO_2-DPA + HNO_2	-162.5	-93.4	
20	DPA+ 2 $^{\bullet}NO_2$ ⟶ 3-NO_2-DPA + HNO_2	-160.3	-94.3	
21	DPA+ 2 $^{\bullet}NO_2$ ⟶ 4-NO_2-DPA + HNO_2	-172.3	-105.8	
	Formation of NNO-DPA			
22	DPA+$^{\bullet}NO_2$ + $^{\bullet}$NO ⟶ ON-N-DPA + HNO_2	-87.3	-27.8	
23	DPA + HNO_2 ⟶ ON-N-DPA + H_2O	-50.8	-43.1	
	Formation of mono-nitroso-DPA (ring-substituted)			
24	DPA+$^{\bullet}NO_2$ + $^{\bullet}$NO ⟶ 2-NO-DPA + HNO_2	-102.7	-38.4	
25	DPA+$^{\bullet}NO_2$ + $^{\bullet}$NO ⟶ 3-NO-DPA + HNO_2	-84.1	-28.8	
26	DPA+$^{\bullet}NO_2$ + $^{\bullet}$NO ⟶ 4-NO-DPA + HNO_2	-100.4	-38.8	
	Electrophilic aromatic substitution of DPA to mono-nitro DPA			
27	DPA + HNO_3 ⟶ 2-NO_2-DPA + H_2O	-125.0	-115.6	Average in ΔH_R and ΔG_R
28	DPA + HNO_3 ⟶ 4-NO_2-DPA + H_2O	-134.8	-128.0	-129.9 / -121.8
29	DPA + N_2O_5 ⟶ 2-NO_2-DPA + HNO_3	-184.4	-174.2	Average in ΔH_R and ΔG_R
30	DPA + N_2O_5 ⟶ 4-NO_2-DPA + HNO_3	-194.3	-186.6	-189.4 / -180.4

No	Reaction type	ΔH_R	ΔG_R	remarks	
	Formation of N-nitroso-mono-nitro DPA from mono-nitro DPA and nitroso DPA				
31	2-N-DPA + $^{\bullet}NO_2$ + $^{\bullet}NO$ ⟶ NNO-2-N-DPA + HNO_2	-55.5	+2.9	small ΔG_R means strong T-dependence	
32	4-N-DPA + $^{\bullet}NO_2$ + $^{\bullet}NO$ ⟶ NNO-4-N-DPA + HNO_2	-73.1	-15.7		
33	NNO-DPA + HNO_3 ⟶ NNO-2-N-DPA + H_2O	-93.3	-86.5		
34	NNO-DPA + HNO_3 ⟶ NNO-4-N-DPA + H_2O	-120.7	-117.4		
	Nitration of mono-nitro DPA to di-nitro-DPA				
35	2-N-DPA + HNO_3 ⟶ 2,2'-DN-DPA + H_2O	-108.9	-100.9		
36	2-N-DPA + HNO_3 ⟶ 2,4'-DN-DPA + H_2O	-124.4	-119.0		
37	2-N-DPA + HNO_3 ⟶ 2,4-DN-DPA + H_2O	-121.0	-116.4		
38	2-N-DPA + HNO_3 ⟶ 2,6-DN-DPA + H_2O	-81.1	-76.3		
39	4-N-DPA + HNO_3 ⟶ 2,4'-DN-DPA + H_2O	-114.5	-106.6		
40	4-N-DPA + HNO_3 ⟶ 4,4'-DN-DPA + H_2O	-125.7	-119.8	Average in ΔH_R and ΔG_R	
41	4-N-DPA + HNO_3 ⟶ 2,4-DN-DPA + H_2O	-111.2	-104.0	-112.8	-106.1
	Nitration of di-nitro DPA to tri-nitro-DPA	Not all reactions are listed here *)			
42	2,4'-DN-DPA + HNO_3 ⟶ 2,4,4'-tri-N-DPA + H_2O	-114.6	-109.5		
43	2,4-DN-DPA + HNO_3 ⟶ 2,4,4'-tri-N-DPA + H_2O	-117.9	-112.1		
44	4,4'-DN-DPA + HNO_3 ⟶ 2,4,4'-tri-N-DPA + H_2O	-103.4	-96.4	Average in ΔH_R and ΔG_R	
45	2,6-DN-DPA + HNO_3 ⟶ 2,6,4'-tri-N-DPA + H_2O	-122.2	-117.1	-102.3	-95.7
	Nitration of tri-nitro DPA to tetra-nitro-DPA	Not all reactions are listed here *)			
46	2,4,4'-tri-N-DPA + HNO_3 ⟶ 2,4,2',4'-tetra-N-DPA + H_2O	-92.9	-85.2	Average in ΔH_R and ΔG_R	
47	2,6,4'-tri-N-DPA + HNO_3 ⟶ 2,6,2',4'-tetra-N-DPA + H_2O	-100.2	-95.1	-93.5	-87.1
	Nitration of tetra-nitro DPA to penta-nitro-DPA	Not all reactions are listed here *)			
48	2,4,2',4'-tetra-N-DPA + HNO_3 ⟶ 2,4,6,2',4'-penta-N-DPA + H_2O	-66.4	-60.5		
49	2,6,2',4'-tetra-N-DPA + HNO_3 ⟶ 2,6,2',4',6'-penta-N-DPA + H_2O	-64.7	-57.5	Average in ΔH_R and ΔG_R	
50	2,6,2',6'-tetra-N-DPA + HNO_3 ⟶ 2,6,2',4',6'-penta-N-DPA + H_2O	-96.7	-91.3	-84.9	-79.5
	Full nitration of DPA in one step				
51	DPA + 6 HNO_3 ⟶ 2,2',4,4',6,6'-hexa-NO_2-DPA + 6 H_2O	-585.9	-544.2	Full nitration in one reaction	
		-97.7	-90.7	per NO_2-group	
	Single nitration from penta-N-DPA				
52	2,4,6,2',6'-penta-N-DPA + HNO_3 ⟶ 2,4,6,2',4',6'-hexa-N-DPA + H_2O	-91.7	-86.8	Average in ΔH_R and ΔG_R	
53	2,4,6,2',4'-penta-N-DPA + HNO_3 ⟶ 2,4,6,2',4',6'-hexa-N-DPA + H_2O	-62.6	-54.4	-77.2	-70.6
	Chemiluminescence, intermediate is an oxidized alkoxy radical				
54	2 NC-ONO_2 ⟶ residual-NC-C=O + residual-NC-OH+ 2 $^{\bullet}NO$+O_2	+53.0	-35.5	From position 2 in NC	
55	2 NC-ONO_2 ⟶ residual-NC-C=O + residual-NC-OH+ 2 $^{\bullet}NO$+O_2	+58.9	-31.1	From position 3 in NC	
56	2 NC-ONO_2 ⟶ residual-NC-C=O + residual-NC-OH+ 2 $^{\bullet}NO$+O_2	+60.1	-25.5	From position 6 in NC	
	For electrophilic aromatic substitution: formation of nitronium cation				
57	N_2O_5 ⟶ NO_2^+ + NO_3^-	$\Delta G^{\ddagger}$ =+115.4 kJ/mol for activation			
58	2 HNO_3 ⟶ H_2O + NO_2^+ + NO_3^-	$\Delta G^{\ddagger}$ =+174.2 kJ/mol for activation			

*) Not all possible reactions are given here for the generation of the higher nitrated products of DPA, see Supplementary Information. But the average values count the average over all possible reactions in the indicated reaction block.

ably the realistic reaction type. This mechanism involves the formation of resonance-stabilized DPA-radical with H radical abstracted from the amino nitrogen. Thereby the ortho and para positions are activated for radical attack by NO_2. After NO_2 addition, the next step is a type of H-atom movement from position 2 or 4 at the ring to the amino nitrogen, which could be similar to any of the multiple hydrogen atom transfers (HAT) mechanisms.

For all these reactions the reaction enthalpies are needed. Because of the lack of literature data the quantum mechanical determination was envisaged. With the program package, Gaussian 2016 the DFT (**D**ensity **F**unctional **T**heo-

Table 8. Selected reactions and their reaction enthalpies ΔH_R in kJ mol^{-1} at 80 °C for use in part 2 [1].

reaction type	$\Delta H_{R,k}$	chosen value	reaction number in Table 7	remark
intrinsic decomposition of NC, NG	$\Delta H_{R,NC}$	−80	1,2,3,4,5,6	to be seen only as 'in between' start value
autocatalytic decomp. of NC, NG	$\Delta H_{R,NC}$	−80	7	to be seen only as 'in between' start value
DPA reacts to NNO-DPA	$\Delta H_{R,NNO}$	−87.3	22	radical reaction, H abstraction by NO_2 and addition of NO
DPA reacts to 4-NO_2-DPA	$\Delta H_{R,4N}$	−134.8	28	electrophilic aromatic substit.
Alternative DPA to 4-NO_2-DPA	$\Delta H_{R,4N}$	−172.3	–	via tautomer, see Table 5
DPA reacts to 2-NO_2-DPA	$\Delta H_{R,2N}$	−125.0	27	electrophilic aromatic substit.
Alternative DPA to 2-NO_2-DPA	$\Delta H_{R,2N}$	−162.5	–	via tautomer, see Table 5
NNO-DPA reacts back to DPA	$\Delta H_{R,DPNNO}$	+87.3	22, reverse	see Table 3, +121.6 in first step
NNO-DPA reacts away	$\Delta H_{R,NNO-}$	−107.0	average of 33, 34	reaction to NNO-mono-nitro DPA and others
4-NO_2-DPA reacts away	$\Delta H_{R,4N-}$	−73.1	32	reaction to NNO-mono-nitro DPA and others
2-NO_2-DPA reacts away	$\Delta H_{R,2N-}$	−55.5	31	reaction to NNO-mono-nitro DPA and others

ry) method was used choosing the functional ωB97X-D and the basis set aug-cc-pvtz to calculate the reaction enthalpies and Gibbs free energies for reaction pathways involving NC, nitroglycerine (NG), and the stabilizer DPA. To have a realistic representation of the molecular environment of the molecules and reactants a polarizable continuum was established around them using the so-called solvation model IEFPCM (**I**ntegral **E**quation **F**ormalism for the **P**olarizable **C**ontinuum **M**odel). The continuum must be characterized by a relative permittivity ε_r, which was set to 7 for the NC continuum. With NC and NG a further technique was applied to enhance the realistic environment by the ONIOM method. (**O**ur own **N**-layered **I**ntegrated molecular **O**rbital and Molecular **M**echanics). It uses identical molecules around the target molecule, and only this central molecule is then calculated on a high DFT level and the outer ones on a reduced but still, good level to save computing time. The reaction enthalpies for NC and NG are quite similar and in the reaction rate schemes, no differentiation was made. For DPA many reactions have been considered and all their reaction enthalpies are reported at 80 °C, which was the temperature of aging and measurement of the DPA consecutive products and the heat flow. These results are used to simulate the heat flow curve of the double-base ball powder K6210, which is demonstrated in the second part of this publication.

7 Supplemental Information

Supplemental information to 'Simulation of Heat Flow curves of NC-based Propellants' Part 1 and Part 2. *Propellants Explosives Pyrotechnics* ***2021***, *46*. DOI: 10.1002/prep.202000314 for Part 1 and DOI: 10.1002/prep.202000313 for Part 2. It can be downloaded as free access. It contains explanations to the QM methods, the thermochemical way to calculate reaction enthalpies, and the list of them calculated for 25 °C.

8 Symbols and Abbreviations

Quantum Mechanical Terms

See also Supplemental Information to this Paper

BLYP	a DFT functional; **B**ecke (gradient corrected exchange potential used in SCF) and **L**ee, **Y**ang, **P**arr (gradient corrected electron correlation potential used in SCF)
D2 dispersion	includes van-der-Waals type dispersion interaction
DFT	(electron) **D**ensity **F**unctional **T**heory
GGA	generalized gradient approximation
H	Hartree energy unit; 1 H = 2625.50 kJ/mol
HF	**H**artee-**F**ock QM method
IEFPCM	**I**ntegral **E**quation **F**ormalism for the **P**olarizable **C**ontinuum **M**odel, a description belonging to the group of so-called SCRF methods (**S**elf-**C**onsistent **R**eaction **F**ield)
NC-continuum	continuum with the relative permittivity of NC. The investigated molecule is situated in a 'cavity' in this continuum
ONIOM	'**O**ur own **N**-layered **I**ntegrated molecular **O**rbital and molecular **M**echanics' model; see https://gaussian.com/oniom technote/
HAT	**H**ydrogen **A**tom **T**ransfer
QM	**Q**uantum **M**echanics
SCF	**S**elf-**C**onsistent **F**ield, an iteration method to determine the minimum energy or best structure (means with minimum energy) or any other property to be optimized
TS	**T**ransition **S**tate

ωB97X-D	also written as wB97XD in Gaussian; long-range corrected version of Becke 97 (B97) functional with exchange and correlation within a hybrid Scheme (X) and empirical Grimme dispersion correction (D) functional
6-31++G(d,p)	basic basis set in Gaussian, applicable from H to Kr, polarizable functions through (3df,3pd), diffuse functions includable by options +,++; see https://gaussian.com/basissets/
aug-cc-pvtz	augmented correlation consistent triple zeta basis; Dunning's correlation consistent basis sets with valence polarization function triple zeta; augmented with additional orbitals: one s, one d, and one p diffuse functions on hydrogen atoms, and one d, one p, one d, and one f diffuse functions on Boron through Neon; see also Supplemental Information to this paper.

Chemical Terms

AHG	anhydroglucose ring (AHG), half of the full monomeric unit cellobiose
sb	single base
db	double base
DN-DPA	di-nitro-DPA
DPA	diphenylamine (stabilizer)
GP	gun propellant
MN-DPA	mono-nitro DPA
NC	nitrocellulose
NG	nitroglycerine, also Ngl
Ngl	nitroglycerine, also NG
P	autocatalytically effective product
$S_{E,Ar}$	electrophilic aromatic substitution
2 N	same as 2 N-DPA (= 2-NO_2-DPA)
2 N-	not further specified product of removal reaction of 2 N
2 N-DPA	2-nitro-diphenylamine, 2-NO_2-DPA
4 N	same as 4 N-DPA (=4-NO_2-DPA)
4 N-	not further specified product of the removal reaction of 4 N
4 N-DPA	4-nitro-diphenylamine, 4-NO_2-DPA
NNO	same as NNO-DPA
NNO-	not further specified product of the removal reaction of NNO
NNO-DPA	N-nitroso-diphenylamine
TriN-DPA	tri-nitro-DPA
TetN-DPA	tetra-nitro-DPA
PenN-DPA	penta-nitro-DPA
ΔH_R	reaction enthalpy
ΔH°_R	reaction enthalpy at standard condition
ΔG_R	reaction Gibbs free energy (Gibbs free energy is also called free enthalpy)
ΔG°_R	reaction Gibbs free energy at standard condition
$\Delta_{bond}H$	bond dissociation enthalpy, also used when formally calculated from dissociation reaction
$\Delta_{bond}G$	bond dissociation Gibbs free energy, also used when formally calculated from dissociation reaction

Acknowledgment

The authors thank Dr. Johannes Lang, Fraunhofer ICT, for hints on the use of quantum mechanical calculation techniques and the calculations of enthalpies of formation of DPA, NNO-DPA, 2-N-DPA, and 4-N-DPA. Dr. Michael Koch from WTD 91 (Bundeswehr Technical Center for Weapons and Ammunition), D-49716 Meppen, Germany is thanked for supporting this work and granting it via BAAINBw, Koblenz. This publication is based on the Bachelor thesis of Mr. Daniel G. Itkis in Chemistry at Ludwig-Maximilian-Universität, München, Germany, referred by Prof. Dr. Klapötke.

Data Availability Statement

The data that support the findings of this study are available in the references given in the paper. References which are not easy to get are available from the corresponding author upon reasonable request.

References

[1] D. G. Itkis, M. A. Bohn, Simulation of Heat Flow Curves of NC-based Propellants-Part 2: Application to DPA stabilized propellants. *Propellants Explos. Pyrotech.* **2021**, *46*, in press. Online published: https://doi.org/10.1002/prep.202000313.

[2] M. J. Frisch, G. W. Trucks, H. B. Schlegel, G. E. Scuseria, M. A. Robb, J. R. Cheeseman, G. Scalmani, V. Barone, G. A. Petersson, H. Nakatsuji, X. Li, M. Caricato, A. V. Marenich, J. Bloino, B. G. Janesko, R. Gomperts, B. Mennucci, H. P. Hratchian, J. V. Ortiz, A. F. Izmaylov, J. L. Sonnenberg, D. Williams-Young, F. Ding, F. Lipparini, F. Egidi, J. Goings, B. Peng, A. Petrone, T. Henderson, D. Ranasinghe, V. G. Zakrzewski, J. Gao, N. Rega, G. Zheng, W. Liang, M. Hada, M. Ehara, K. Toyota, R. Fukuda, J. Hasegawa, M. Ishida, T. Nakajima, Y. Honda, O. Kitao, H. Nakai, T. Vreven, K. Throssell, J. A. Montgomery, Jr., J. E. Peralta, F. Ogliaro, M. J. Bearpark, J. J. Heyd, E. N. Brothers, K. N. Kudin, V. N. Staroverov, T. A. Keith, R. Kobayashi, J. Normand, K. Raghavachari, A. P. Rendell, J. C. Burant, S. S. Iyengar, J. Tomasi, M. Cossi, J. M. Millam, M. Klene, C. Adamo, R. Cammi, J. W. Ochterski, R. L. Martin, K. Morokuma, O. Farkas, J. B. Foresman, D. J. Fox. Gaussian 16 Revision C.01, 2016. Gaussian Inc. Wallingford CT 06492, USA. https://gaussian.com/g16new/.

[3] J.-D. Chai, M. Head-Gordon, Long-range corrected hybrid density functionals with damped atom-atom dispersion corrections. *Phys. Chem. Chem. Phys.* **2008**, *10*, 6615–6620. https://doi.org/10.1039/B810189B.

[4] A. D. Becke, Density-functional thermochemistry. V. Systematic optimization of exchange-correlation functionals. *J. Chem. Phys. 107* (**1997**) 8554–8560. https://doi.org/10.1063/1.475007.

[5] S. Grimme, Semiempirical GGA-type density functional constructed with a long-range dispersion correction. *J. Comput. Chem.* **2006**, *27*, 1787–1799. https://doi.org/10.1002/jcc.20495.

[6] R. K. Raju, A. A. Bengali, E. N. Brothers, A unified set of experimental organometallic data used to evaluate modern theoretical methods. *Dalton Trans.* **2016**, *45*, 13766–13778. https://doi.org/10.1039/C6DT02763F.

[7] L. A. Burns, Á. Vázquez-Mayagoitia, B. G. Sumpter, C. D. Sherril, Density-functional approaches to non-covalent interactions: A comparison of dispersion corrections (DFT-D), exchange-hole dipole moment (XDM) theory, and specialized functionals. *J. Chem. Phys.* **2011**, *134*, 084107. DOI: https://doi.org/10.1063/1.3545971.

[8] S. Miertuš, E. Scrocco, J. Tomasi, Electrostatic interaction of a solute with a continuum. A direct utilization of ab initio molecular potentials for the prevision of solvent effects. *Chem. Phys.* **1981**, *55*, 117–129. DOI: https://doi.org/10.1016/0301-0104(81)-85090-2.

[9] J. Quinchon, J. Tranchant, Nitrocelluloses: the materials and their applications in propellants, explosives and other industries. *Ellis Horwood* **1989**.

[10] S. Dapprich, I. Komáromi, K. S. Byun, K. Morokuma, M. J. Frisch, A new ONIOM implementation in Gaussian98. Part I: The calculation of energies, gradients, vibrational frequencies, and electric field derivatives. *Journal of Molecular Structure: THEOCHEM* **1999**, *461–462*, 1–21. https://doi.org/10.1016/S0166-1280(98)-00475-8.

[11] T. B. Brill, P. E. Gongwer, Thermal Decomposition of Energetic Materials 69. Analysis of the Kinetics of Nitrocellulose at 50 °C to 500 °C. *Propellants Explos. Pyrotech.* **1997**, *22*, 38–44. https://doi.org/10.1002/prep.19970220109.

[12] M. A. Bohn, Bond Dissociation Enthalpies of the CO–NO2 Bonds in Nitric Acid Ester Groups and in Peroxo-nitrite and Peroxo-nitrate Groups Determined by DFT Calculations. *Proceedings of the 39th International Annual Conference of ICT* on 'Energetic Materials – Processing and Product Design', June 24 to 27, 2008, Karlsruhe, Germany. *Pages 71–1 to 71–12*. Proceedings by Fraunhofer-Institut für Chemische Technologie (ICT), D-76318 Pfinztal-Berghausen, Germany, **2008**. ISSN 0722–4087. Typo-corrected version by 11 Nov **2020**.

[13] A. Pfeil, H. H. Krause, N. Eisenreich, The consequences of beginning slow thermal decomposition on the molecular weight of nitrated cellulose. *Thermochim. Acta* **1985**, *85*, 395–398. https://doi.org/10.1016/0040-6031(85)85608-2.

[14] F. Volk, M. A. Bohn, G. Wunsch, Determination of Chemical and Mechanical Properties of Double-Base Propellants during Ageing. *Propellants Explos. Pyrotech.* **1987**, *12*, 81–87. https://doi.org/10.1002/prep.19870120305.

[15] M. A. Bohn, F. Volk, Sicherheits- und Funktionsbewertung von Treibmitteln durch Messen von Wärmeentwicklung, Stabilisatorverbrauch und Molmassenabbau. (Safety and functional assessment of propellants by measuring of heat flow, stabilizer consumption and molar mass degradation). Paper 65 *on 21st International Annual Conference of ICT on 'Technology of Polymer Compounds and Energetic Materials'*, 3–6 July 1990, Karlsruhe Germany. Pages 65–1 to 65–19 in conference proceedings, edited by Fraunhofer Institut für Chemische Technologie (ICT), D-76318 Pfinztal-Berghausen, Germany, **1990**. ISSN 0722–4087.

[16] M. A. Bohn, F. Volk, Aging Behavior of Propellants Investigated by Heat Generation, Stabilizer Consumption, and Molar Mass Degradation. *Propellants Explos. Pyrotech.* **1992**, *17*, 171–178. https://doi.org/10.1002/prep.19920170405.

[17] M. L. Wolfrom, J. H. Frazer, L. P. Kuhn, E. E. Dickey, S. M. Olin, D. O. Hoffman, R. S. Bower, A. Chaney, Eloise Carpenter, P. McWain, The Controlled Thermal Decomposition of Cellulose Nitrate. *J. Am. Chem. Soc.* **1955**, *77*, 6573–6580. https://doi.org/10.1021/ja01629a045.

[18] R. W. Phillips, Ch. A. Orlick, Rudolph Steinberger, The Kinetics of the Thermal Decomposition of Nitrocellulose. *J. Phys. Chem.* **1955**, *59*, 1034–1039. https://doi.org/10.1021/j150532a011.

[19] M. A. Hiskey, K. R. Brower, J. C. Oxley, Thermal Decomposition of Nitrate Esters. *J. Phys. Chem.* **1991**, *95*, 3955–3960. https://pubs.acs.org/doi/pdf/10.1021/j100163a013.

[20] H. N. Volltrauer, A. Fontijn, Low-temperature pyrolysis studies by chemiluminescence techniques real-time nitrocellulose and PBX 9404 decomposition. *Combust. Flame* **1981**, *41*, 313–324. https://doi.org/10.1016/0010-2180(81)90065-1.

[21] J. Kimura, Chemiluminescence Study on Thermal Decomposition of Nitrate Esters (PETN and NC). *Propellants Explos. Pyrotech.* **1989**, *14*, 89–92. https://doi.org/10.1002/prep.19890140302.

[22] J. Kimura, Kinetic Mechanism on Thermal Degradation of a Nitrate Ester Propellant. *Propellants Explos. Pyrotech.* **1988**, *13*, 8–12. https://doi.org/10.1002/prep.19880130103.

[23] W. Swientosławski, Thermochemische Untersuchungen der organischen Verbindungen. Dritte Mitteilung. Stickstoffhaltige Verbindungen. (Thermochemical investigations of organic compounds. Third communication. Nitrogen containing compounds). *Zeitschrift für Physikalische Chemie* **1910**, *72*, 49–83. https://doi.org/10.1515/zpch-1910-7205.

[24] F. Volk, Determining the Shelflife of Solid Propellants. *Propellants Explos. Pyrotech.* **1976**, *1*, 59–65. https://doi.org/10.1002/prep.19760010305.

[25] N. J. Curtis, P. E. Rogasch, Determination of Derivatives of Diphenylamine in Australian Gun Propellants by High Performance Liquid Chromatography. *Propellants Explos. Pyrotech.* **1987**, *12*, 158–163. https://doi.org/10.1002/prep.19870120505.

[26] N. J. Curtis, Isomer distribution of nitro derivatives of diphenylamine in gun propellants: Nitrosamine Chemistry. *Propellants Explos. Pyrotech.* **1990**,*15*, 222–230. https://doi.org/10.1002/prep.19900150509.

[27] M. N. Boers, W. P. C. de Klerk, Lifetime Prediction of EC, DPA, Akardite II and MNA Stabilized Triple Base Propellants, Comparison of Heat Generation Rate and Stabilizer Consumption. *Propellants Explos. Pyrotech.* **2005**, *30*, 356–362. https://doi.org/10.1002/prep.200500026.

[28] M. A. Bohn, N. Eisenreich, Kinetic Modelling of the Stabilizer Consumption and of the Consecutive Products of the Stabilizer in a Gun Propellant. *Propellants Explos. Pyrotech.* **1997**, *22*, 125–136. https://doi.org/10.1002/prep.19970220306.

[29] A. Alm, *Studies on Reactions Between Nitrogen Oxides and Diphenylamine Compounds. Proceed. 1st Symposium on 'Chemical Problems Connected with the Stability of Explosives'* (Symposium held in Stockholm, May 22–23, 1967), pages 179–187. Editor: Jan Hansson, **1968**, Stockholm, Sweden.

[30] L.-S. Lussier, H. Gagnon, M. A. Bohn, On the Chemical Reactions of Diphenylamine and its Derivatives with Nitrogen Dioxide at Normal Storage Temperature Conditions . *Propellants Explos. Pyrotech.* **2000**, *25*, 117–125. https://doi.org/10.1002/1521-4087(200006)25:3<117::AID-PREP117>3.0.CO;2-8.

[31] T. Lindblom, Reactions in Stabilizer and Between Stabilizer and Nitrocellulose in Propellants. *Propellants Explos. Pyrotech.* **2002**, *27*, 197–208. https://doi.org/10.1002/1521-4087(200209)-27:4<197::AID-PREP197>3.0.CO;2-W.

[32] A. Chin, D. S. Ellison, S. K. Poehlein, M. K. Ahn, Investigation of the Decomposition Mechanism and Thermal Stability of Nitrocellulose/Nitroglycerine Based Propellants by Electron Spin Resonance. *Propellants Explos. Pyrotech.* **2007**, *32*, 117–126. https://doi.org/10.1002/prep.200700013.

[33] R. C. Mowrey, M. Page, G. F. Adams B. H. Lengsfield III, Ab initio multireference configuration interaction study of CH_2NNO_2. HONO elimination vs NN bond fragmentation. *J. Chem. Phys.* **1990**, *93*, 1857–1864. https://doi.org/10.1063/1.459063.

[34] R. W. Molt, T. Watson, A. P. Bazanté, R. J. Bartlett, N. G. J. Richards, Gas phase RDX decomposition pathways using coupled cluster theory. *Phys. Chem. Chem. Phys.* **2016**, *18*, 26069–26077. https://doi.org/10.1039/C6CP05121A.

[35] T.-L. Su, Christos Christodoulatos, Destruction of nitrocellulose using alkaline hydrolysis. Technical report 1996. Center for Environmental Engineering, *Stevens institute of Technology, Hoboken NJ, USA.* **1996**. https://apps.dtic.mil/sti/pdfs/ADP017728.pdf.

[36] R. A. Fifer, Chemistry of nitrate ester and nitramine propellants. In *Fundamentals of solid-propellant combustion, volume 90, page 177*. Progress in Astronautics and Aeronautics Series, **1984**. https://doi.org/10.2514/5.9781600865671.0177.0237.

[37] T. Lindblom, Reactions in the system Nitrocellulose/Diphenylamine with special reference to the formation of a stabilizing product bonded to nitrocellulose. *PhD thesis, University of Uppsala*, April **2004**. http://www.diva-portal.org/smash/get/diva2:164030/FULLTEXT01.pdf.

[38] R. Wei, S. Huang, Z. Wang, Ch. Wang, T. Zhou, J. He, R. Yuen, J. Wang, Effect of plasticizer dibutyl phthalate on the thermal decomposition of nitrocellulose. *J. Therm. Anal. Calorim.* (**2018**, *134*, 953–969. https://doi.org/10.1007/s10973-018-7653-5.

[39] S. Hammes-Schiffer, Proton-Coupled Electron Transfer: Moving Together and Charging Forward. *J. Am. Chem. Soc.* **2015**, *137*, 8860–8871. https://doi.org/10.1021/jacs.5b04087.

[40] J. J. Warren, J. M. Mayer, Predicting organic hydrogen atom transfer rate constants using the Marcus cross relation. *Proc.-Nat.Acad.Sci.USA (PNAS)* **2010**, *107*, 5282–5287. https://doi.org/10.1073/pnas.0910347107.

[41] R. Tyburski, T. Liu, S. D. Glover, L. Hammarström, Proton-Coupled Electron Transfer Guidelines, Fair and Square. *J. Am. Chem. Soc.* **2021**, *143*, 560–576. https://dx.doi.org/10.1021/jacs.0c09106.

Manuscript received: December 3, 2020
Revised manuscript received: April 29, 2021
Version of record online: June 30, 2021

